Journal of Medicinal Chemistry

pubs.acs.org/jmc

Article

Serum-Stable Gold(III) Bisphosphine Complex Induces Mild Mitochondrial Uncoupling and In Vivo Antitumor Potency in Triple Negative Breast Cancer

Adedamola S. Arojojoye, Chibuzor Olelewe, Sailajah Gukathasan, Jong H. Kim, Hemendra Vekaria, Sean Parkin, Patrick G. Sullivan, and Samuel G. Awuah*

Cite This: *J. Med. Chem.* 2023, 66, 7868−7879

Read Online

ACCESS | Metrics & More | Article Recommendations | Supporting Information

ABSTRACT: The preparation of cyclometalated complexes offers a path to stable materials, catalysts, and therapeutic agents. Here, we explore the anticancer potential of novel biphenyl organogold(III) cationic complexes supported by diverse bisphosphine ligands, **Au-1**−**Au-5**, toward aggressive glioblastoma and triple negative breast cancer cells (TNBCs). The [C^C] gold(III) complex, **Au-3**, exhibits significant tumor growth inhibition in a metastatic TNBC mouse model. Remarkably, **Au-3** displays promising blood serum stability over a relevant therapeutic window of 24 h and alteration in the presence of excess *L*-GSH. The mechanism-of-action studies show that **Au-3** induces mitochondrial uncoupling, membrane depolarization, and G1 cell cycle arrest and prompts apoptosis. To the best of our knowledge, **Au-3** is the first biphenyl gold-phosphine complex to uncouple mitochondria and inhibit TNBC growth in vivo.

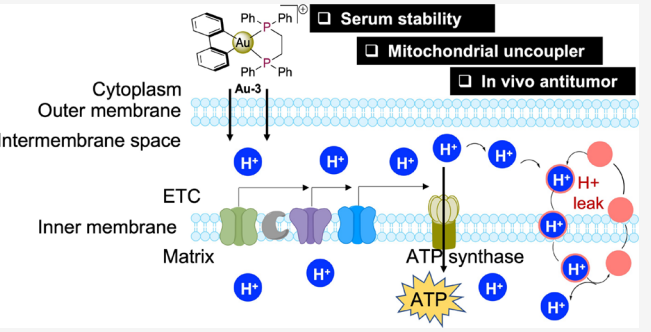

INTRODUCTION

Cancer remains one of the most difficult diseases to treat and is associated with high mortality rates.[1,2] The spectrum of available effective drugs is still limited with some presenting acute toxicity and severe side effects,[3−5] therefore developing new drugs and treatment options are desperately needed. Gold-based complexes represent a promising class of bioactive agents with remarkable anticancer potential.[6−8] Ongoing research toward repurposing auranofin for various diseased conditions in the clinic[9,10] has stimulated the development and elucidation of different gold-derived anticancer agents and their mode of drug action.

Structural modifications to gold-containing scaffolds result in complexes manifested by changes in oxidation states, geometry, and different chelating ligands to stabilize the gold center.[11−17] Notable work includes the development of mitochondrial targeting Au(I)-NHCs and Au(I)-$(DPPE)_2Cl$ that showed high cytotoxicity against cancer cells in vitro and in vivo but failed in preclinical toxicity studies.[18,19] Furthermore, Au(III)-dithiocarbamate complexes trigger proteosome inhibition and potent in vivo effects.[20] Gold porphyrin is another class of Au(III) complexes with an excellent cytotoxic profile in a panel of cancer cells and inhibited tumor growth in mice with multiple mechanisms of action depending on the tetranitrogenic porphyrin ligand used.[21−24] To resolve the existing problem of Au(III) complex instability, we and others have used cyclometalation as a strategy to improve compound stability in solution.[25−29] Recent speciation studies using chiral Au(III) complexes with glutathione deepened our understanding into Au(III) stability; however, enhanced complex stability will facilitate clinical translation of gold therapeutic agents.[30] The use of [C^C]-cyclometalation demonstrated stability for use as catalysts and as luminescent agents.[31−35] Recently, [C^C]Au(III)-bearing bidentate ligands were shown to exhibit cytotoxic activity in cancer cells; however, their biological target and the mechanism-of-action studies were not fully elucidated.[36]

Bisphosphines are diverse bidentate ligands that have found widespread use in coordination chemistry, homogeneous transition metal-catalyzed organic reactions, and in biological systems.[37] Early work on the preparation of cytotoxic gold complexes bearing bisphosphines by Berners-Price, Sadler, and Mirabelli[18,38−41] followed by other synthetic efforts to develop bisphosphine-supported gold agents have highlighted their importance as possible chemotherapeutics.[42−47] Darkwa et al., and Raubenheimer et al., independently studied the effect of

Received: February 11, 2023
Published: June 6, 2023

the nature of phosphine ligands on the anticancer properties of phosphinogold(I) complexes. They rationalized that the substituent on the phosphorus atom dictates the anticancer activity. Bisphosphine complexes with longer CH_2 linkers demonstrate better anticancer properties than complexes with shorter CH_2 linkers.[48,49] However, their mechanism of cytotoxic action was not fully discussed.

Reducing the efficiency of energy conversion while maintaining high intracellular phosphate levels in the mitochondria is known as mitochondrial uncoupling.[50−53] Pharmacological induction of mild mitochondrial uncoupling has been used to control obesity, atherosclerosis, diabetes, fatty liver disease, and more recently cancer by dinitrophenol (DNP) and its derivatives.[50,54−57] Thus, novel small molecules that induce mitochondrial uncoupling can alter cancer cell metabolism, energy homeostasis, and mitochondria-dependent apoptosis toward clinically relevant targeted therapy. Earlier reports on $[Au(I)\text{-}(DPPE)_2]^+$ have shown that they induce uncoupling of mitochondrial oxidative phosphorylation by enhanced permeability of the inner mitochondrial membrane to cations in isolated rat liver mitochondria.[58,59] We hypothesized that stable redox-active Au(III) cations interact with mitochondria to enhance electron flux, leading to mitochondrial uncoupling.

Here, we prepared biphenyl Au(III) complexes bearing bisphosphine ligands with significant serum and solution stability as well as mild mitochondrial uncoupling activity to disrupt mitochondrial energy states. The complexes possess potent anticancer activity in multiple aggressive cancer cells including TNBC and glioblastoma cells and inhibit TNBC tumor growth in vivo. To our prime knowledge, this is the first account of Au(III) complexes to induce mitochondrial uncoupling and inhibit tumor growth in vivo.

RESULT AND DISCUSSION

Synthesis and Characterization. We rationalized that the μ-chloro biphenyl Au(III)[33,35,60] could be a readily accessible building block to preparing bisphosphine-substituted organogold complexes of the archetype, $[[C\text{^}C]Au(III)P{-}P]^+$. The synthetic protocol is amenable to different bisphosphine ligands such as quinoxaline frameworks with or without a chiral phosphanyl side chain (**Au-1** or **Au-4**) or an aromatic backbone with an aromatic phosphanyl side chain (**Au-2** and **Au-5**) and an aromatic backbone with aliphatic phosphanyl side chains (**Au-3**) in moderate yields (Figure 1A).

All synthesized gold complexes were characterized by ^1H NMR, ^{31}P NMR, and ^{13}C NMR; EA and purity were assessed by high-performance liquid chromatography (HPLC) and found to be greater than 97%. Single crystals of complexes were resolved by X-crystallography either with chloride anions (**Au-1**, **Au-2**) or $[C\text{^}C]Au(III)Cl_2$ anions (**Au-2a**, **Au-3a**) to elucidate the structure of the complexes (Figures 1B and S1−S4). Electrochemical characterization of representative complexes (**Au-2** and **Au-3**) by cyclic voltammetry in acetonitrile revealed low redox potentials with a reduction peak at −1.14 V and oxidation events at 0.65−0.79 V using Ag/AgCl reference electrodes (Figures 1C and S30−S33).

Physiological Stability Studies. Evidence for physiological stability of **Au-1**−**Au-5** was established using systematic UV−vis spectroscopy, APCI-MS, or LC-ESI-MS methods (Figures 2 and S34−S61). First, UV−vis spectroscopic monitoring of the reaction of the complexes (100 μM) with L-GSH (1000 μM) showed unaltered high energy charge

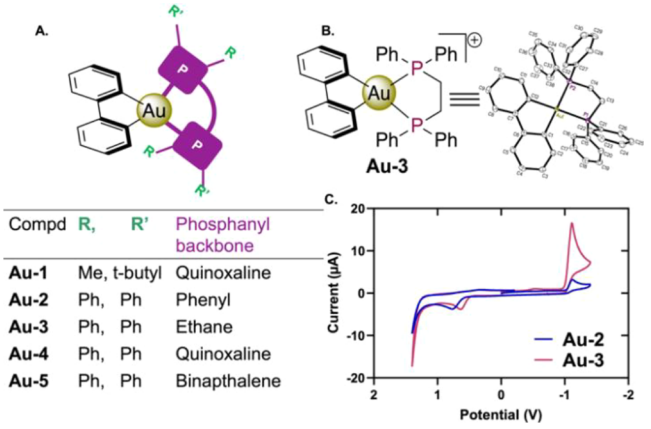

Compd	R,	R'	Phosphanyl backbone
Au-1	Me,	t-butyl	Quinoxaline
Au-2	Ph,	Ph	Phenyl
Au-3	Ph,	Ph	Ethane
Au-4	Ph,	Ph	Quinoxaline
Au-5	Ph,	Ph	Binapthalene

Figure 1. A. Generic chemical structure of biphenyl Au(III) complexes showing bisphosphine ligands used in this work B. Chemical structure of **Au-3** used in this work and the ORTEP representation of **Au-3** (biphenyl $AuCl_2$ anion omitted for clarity). CCDC no: 2233442 C. Cyclic voltammogram of **Au-2** and **Au-3** at 0.1 V/s with the Ag/AgCl reference electrode.

transfer transitions over 24 h for all complexes except **Au-5**. Complexes **Au-2** and **Au-3** show absorption peaks at ∼250 nm and ∼ 350 nm, respectively, over 24 h. (Figures 2A, 4B and S41−S59). Further MS analysis of the reaction between *L*-GSH with **Au-1**−**Au-5** in an equimolar ratio by APCI-MS confirmed that no quantitative adduct was formed. For instance, **Au-2** and **Au-3** showed peaks with m/z = 794.5 [**Au-2**] and 746.5 [**Au-3**] corresponding to $[M\text{-}Cl]^+$ peaks dominant after 8 h of reaction with no interaction with *L*-GSH m/z = 307.8 (Figures 2A and S41−S59). Second, a more translational stability study was performed by incubating **Au-3** in murine blood serum for 24 h. Quantitative decay plots using LC-ESI-MS show that more than 60% of the complex remain intact, suggesting that majority of **Au-3** may remain intact in circulation until it reaches its site of action (Figure 2B).

In Vitro Cytotoxicity and Cellular Uptake. Several cyclometalated Au(III) complexes have been shown to induce significant antiproliferative activity by apoptosis or autophagy.[61−64] We expected that **Au-1**−**Au-5** recapitulate these features. **Au-1**−**Au-5** showed lower IC_{50} values compared to cisplatin (a first-line chemotherapeutic drug) in the panel of cancer cells studied: MDA-MB-468 and MDA-MB-231 (human breast cancer), 4T1 (murine breast cancer), and BT333 (human glioblastoma) 72 h post-treatment by MTT (Table 1, Figures S60−S65).

Apoptosis and Cell Cycle Analysis. Evidence for apoptosis came from a fluorescence-assisted cell sorting (FACS) study using the TNBC cells MDA-MB-468 cells exposed to 0.1 or 0.3 μM of **Au-3** along with Annexin-V-FITC and propidium iodide (Figure 3A). From the study, it was inferred that cells treated with **Au-3** induced 17.4 and 31.6% apoptosis at 0.1 and 0.3 μM, respectively, in MDA-MB-468 cells after 48 h of exposure when compared to control cells. A similar trend was observed for MDA-MB-231 cells (Figure S66). To analyze the effect of **Au-3** on the DNA content, FACS studies revealed marginal cell cycle arrest with an 8% increase of the G0/G1 phase in MDA-MB-468 at 1 μM in a dose-dependent fashion after 12 h post treatment (Figure 3B). This finding coupled with our design principle of a stable lipophilic cation led us to suggest that **Au-3** may target mitochondria and disrupt metabolic pathways.

https://doi.org/10.1021/acs.jmedchem.3c00238
J. Med. Chem. 2023, 66, 7868−7879

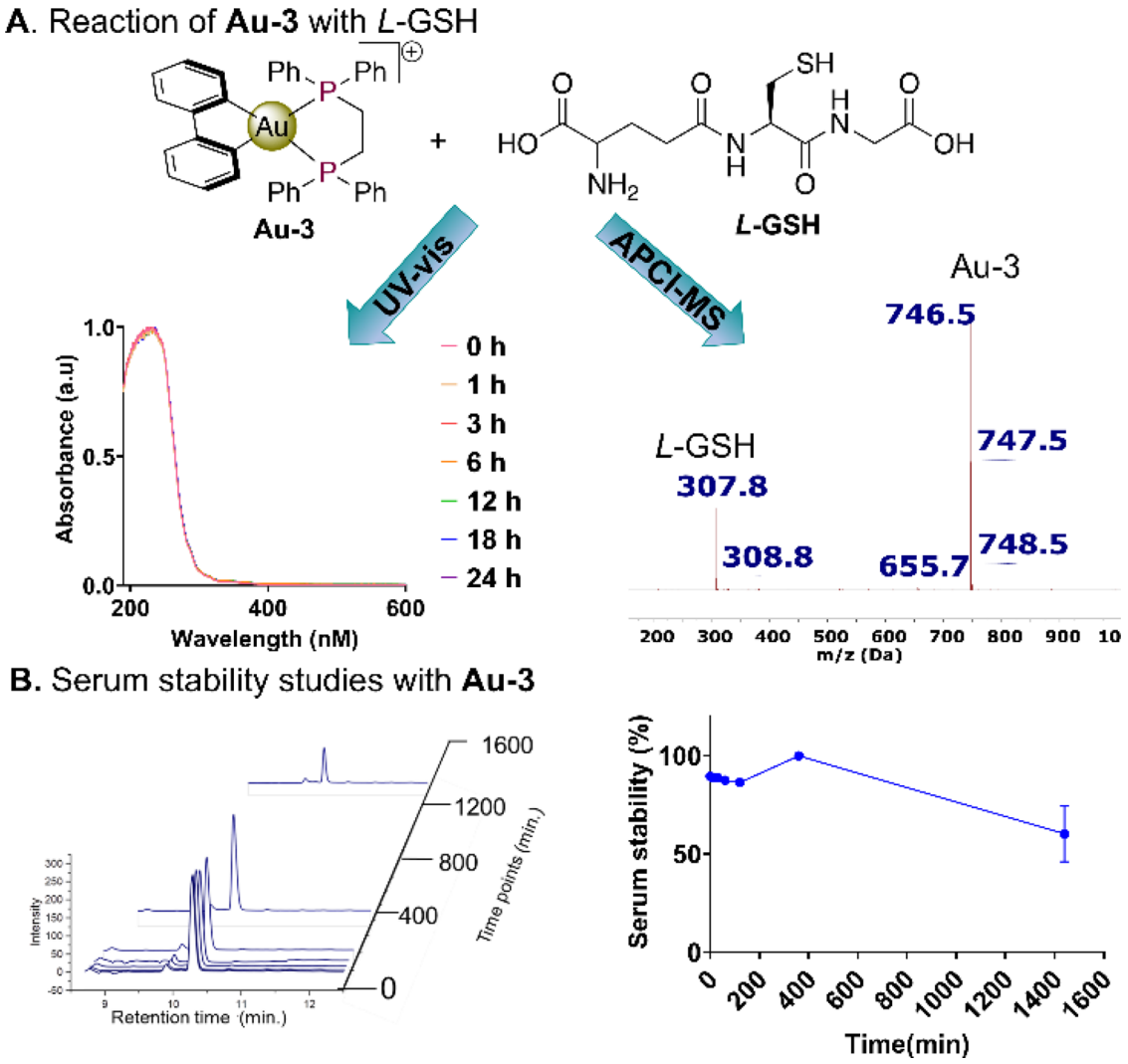

Figure 2. Physiological stability studies. **A**. Reaction of **Au-3** with *L*-glutathione using UV−vis (24 h) and APCI-MS (8 h) **B**. LC-ESI-MS serum stability studies of **Au-3** (100 μM, 24 h) and decay plot (right) extrapolated from HPLC AUC (left).

Table 1. Table Showing IC_{50} Values (μM) for Complex Au-1−Au-5 and Cisplatin, in MDA-MB-468, MDA-MB-231, 4T1, and BT-333 Cancer Cells[a]

compounds	MDA-MB-468	MDA-MB-231	4T1	BT-333
Au-1	0.11 ± 0.12	0.49 ± 0.06	0.85 ± 0.18	0.76 ± 0.08
Au-2	0.21 ± 0.14	0.25 ± 0.21	1.18 ± 0.16	0.93 ± 0.09
Au-3	0.11 ± 0.09	0.55 ± 0.09	0.38 ± 0.2	0.52 ± 0.07
Au-4	0.33 ± 0.18	0.20 ± 0.18	0.13 ± 0.08	1.43 ± 0.12
Au-5	6.76 ± 0.65	2.62 ± 0.25	2.07 ± 0.27	3.38 ± 0.04
cisplatin	2.60 ± 0.61	43.14 ± 0.9[a]	1.0 ± 0.17[a]	23.2 ± 0.29

[a]Reported IC_{50} values of cisplatin in MDA-MB-231 and 4T1.[65,66]

Au-3 Induces Mitochondria Uncoupling Activity in TNBC Cells. Mitochondrial uncoupling can be characterized by key biochemical hallmarks including (i) increase in oxygen consumption even at the inhibition of ATP synthase, (ii) reduction in mitochondrial potential, and (iii) decrease in mitochondrial ATP production. These among others destabilize cellular energy homeostasis and create an exploitable vulnerability for relevant cancer treatment.

We initially tested whether **Au-3** would promote the oxygen consumption rate (OCR) in a Mitostress test using Seahorse XF96. In isolated mitochondria from C57BL/6J mice, a concentration-dependent increase in OCR at state IV respiration (Figure 3C) was observed even when ATP synthase was inhibited by oligomycin indicative of uncoupling activity. Additionally, in cancer cells where the membrane potential is more negative to drive accumulation of lipophilic cation complexes such as **Au-3**, the complex induced increased OCR in MDA-MB-468 cells. As inferred from the maximal respiration in the presence of oligomycin (Figure 3D,E) and extrapolated proton leak (Figure 3F), significant increase in OCR up to 2.7 μM with concomitant decrease in the coupling efficiency confirmed mitochondrial uncoupling (Figure 3G).

https://doi.org/10.1021/acs.jmedchem.3c00238
J. Med. Chem. 2023, 66, 7868−7879

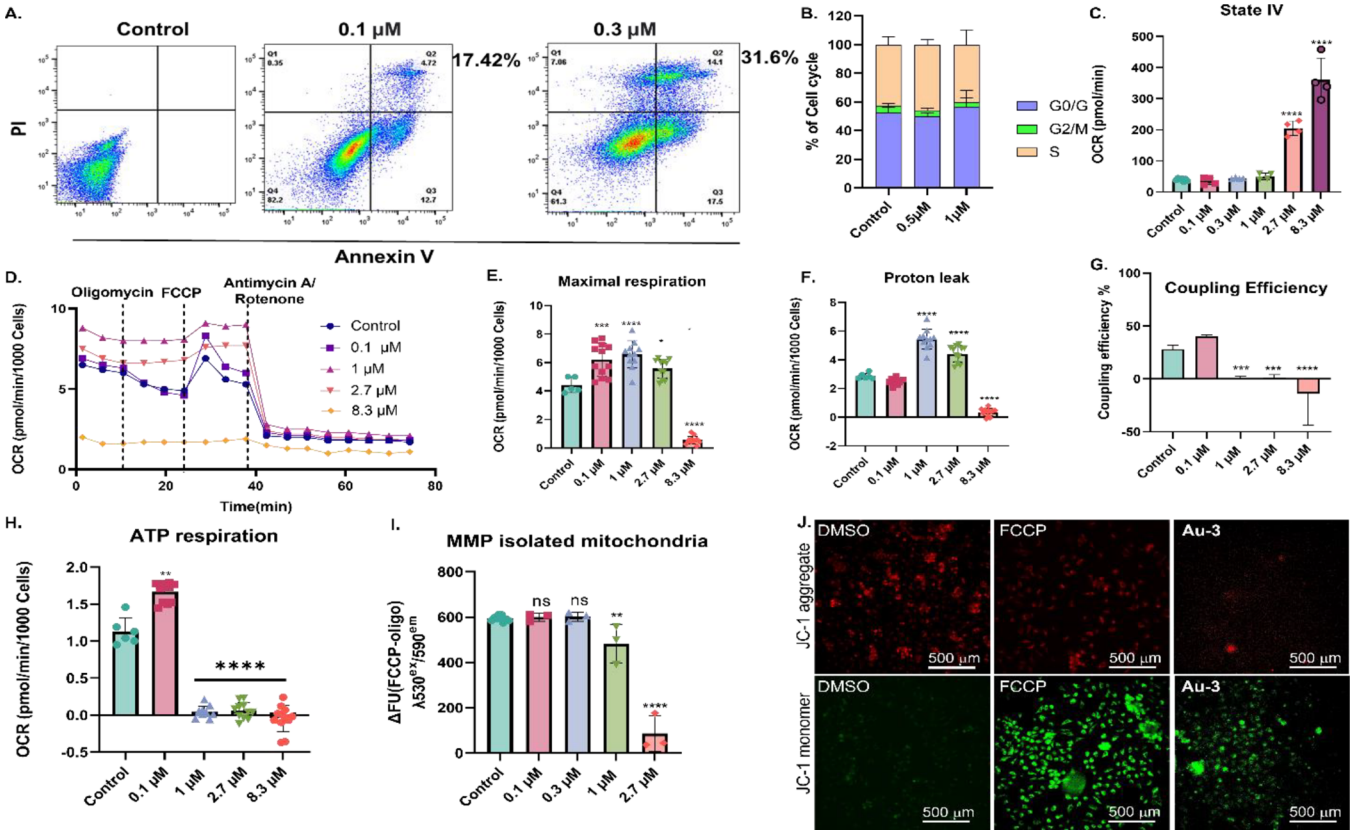

Figure 3. Mechanistic studies on the mode of action of **Au-3**. (A) Flow cytometry result showing apoptosis at 0.1 and 0.3 μM in MDA-MB-468 cells. (B) Cell cycle analysis of **Au-3** at 0.5 and 1 μM. (C) Extrapolated state IV data from isolated mitochondria of C57BL/6J mice. (D) MitoStress study using Seahorse assay. MDA-MB-468 cancer cells were pretreated with **Au-3** (12 h) and various inhibitors of ETC were added at indicated time points. (E−H) Key parameters extrapolated from Seahorse assay. (I) Mitochondria membrane potential of isolated mitochondria of C57BL/6J mice using TMRE dye. (J) Mitochondria membrane potential of MDA-MB-468 using JC-1 dye. **Au-3** was administered at (10 μM) for 90 min. Ordinary one-way ANOVA *p < 0.05, ** p < 0.1, ***p < 0.001, ****p < 0.0001.

The highest **Au-3** concentration of 8.3 μM induced stress in cancer cells that shut down the ETC compared to effects on healthy mitochondria, depicting selectivity.

Next, levels of respiratory-linked ATP were assessed in MDA-MB-468 cells incubated with **Au-3** compared to vehicle control cells. Following an initial burst in ATP production at 0.1 μM of **Au-3**, higher dose treatments of 1−8.3 μM resulted in total abrogation of ATP production, which is the energy currency of the cell (Figure 3H).

To test whether the mitochondria uncoupling activity induced by **Au-3** was independent of cytotoxic action or cellular stress, we investigated the uncoupling potential of the cytotoxic platinum drug, cisplatin in MDA-MB-468 cells. Briefly, cells were treated with varying concentrations of cisplatin for 12 h. Following the 12 h pre-treatment period, the mitostress test was performed as previously described, and we observed that cisplatin did not alter OCR significantly. Extrapolated maximal respiration, proton leak, and coupling efficiency data (Figure S70A−E) support this finding. Clearly, **Au-3**-induced mitochondria uncoupling activity is differentiated from cisplatin, and the characteristic uncoupling phenotype is consistent with the hypothesis put forth.

Another crucial phenotype of uncoupler-induced cytotoxicity is the loss of mitochondrial membrane potential ($\Delta\psi_m$). Using fluorescence-based assays, we assessed whether Au-3 depolarized $\Delta\psi_m$. **Au-3**-induced depolarization in isolated mitochondria in a concentration-dependent manner from 0.1 to 2.7 μM along with TMRE (tetramethylrhodamine, ethyl ester), which labels active mitochondria via a plate reader (Figure 3I). The depolarized phenotype was recapitulated in live MDA-MB-468 cells using JC-1 assay via microscopy. The treatment of MDA-MB-468 with 10 μM led to green JC-1 monomers, indicative of mitochondrial depolarization (Figure 3J).

Structure−Activity Relationship Considerations. We further carried out a detailed structure−activity relationship (SAR) study on **Au-1**−**Au-5** to understand the effect of phosphanyl side groups and backbone on their cellular responses. First, theoretical Log$P$ values of **Au-1**−**Au-5** were computed using SWISSADME software.[67] **Au-1** with aliphatic t-butyl and methyl phosphanyl side groups displayed the lowest lipophilicity (Log$P$ = 4.88) and **Au-2**-**Au-5** with phenyl side groups displayed high lipophilicity (Log$P$ = 6.38−>10). Although **Au-1** and **Au-4** differ only in the nature of side groups attached to the quinoxaline phosphanyl backbone, they display great differences in lipophilicity, as shown in Figure 4A. Also, within complexes with phenyl side groups, **Au-3** with an aliphatic nonconjugated backbone has the lowest Log$P$ value while **Au-5** with increased conjugated binaphthyl backbone displayed a Log$P$ value greater than 10. Second, solution stability studies of **Au-1**−**Au-5** in DMEM or GSH also showed that complexes with aliphatic phosphanyl side groups (**Au-1**) or backbone **Au-3** were more stable compared to complexes

https://doi.org/10.1021/acs.jmedchem.3c00238
J. Med. Chem. 2023, 66, 7868−7879

A.

Complexes	LogP
Au-1	4.88
Au-2	6.92
Au-3	6.38
Au-4	>10
Au-5	>10

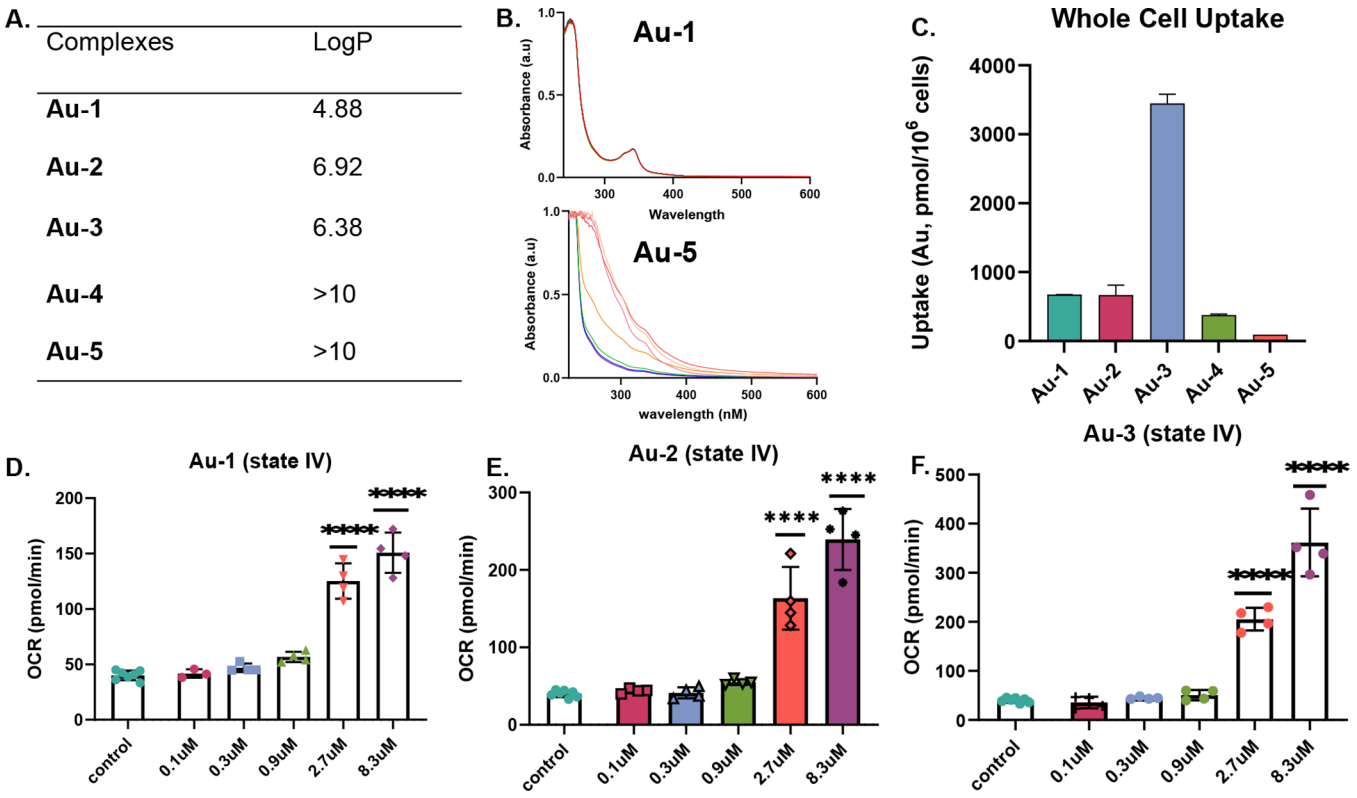

Figure 4. SAR studies. (A) Theoretical Log*P* values of **Au-1**−**Au-5** computed from SWISSADME software. (B) UV−vis solution stability studies of **Au-1** (top) and **Au-5** (bottom) over 24 h. (C) Intracellular accumulation of **Au-1**−**Au-5** in MDA-MB-468 cancer cells. Cells were treated with 10 μM for 18 h. (D−F) Extrapolated state IV data from treatment of **Au-1**−**Au-3** on isolated mitochondria of C57BL/6J mice. Ordinary one-way ANOVA *p < 0.05, **p < 0.1, ***p < 0.001, ****p < 0.0001.

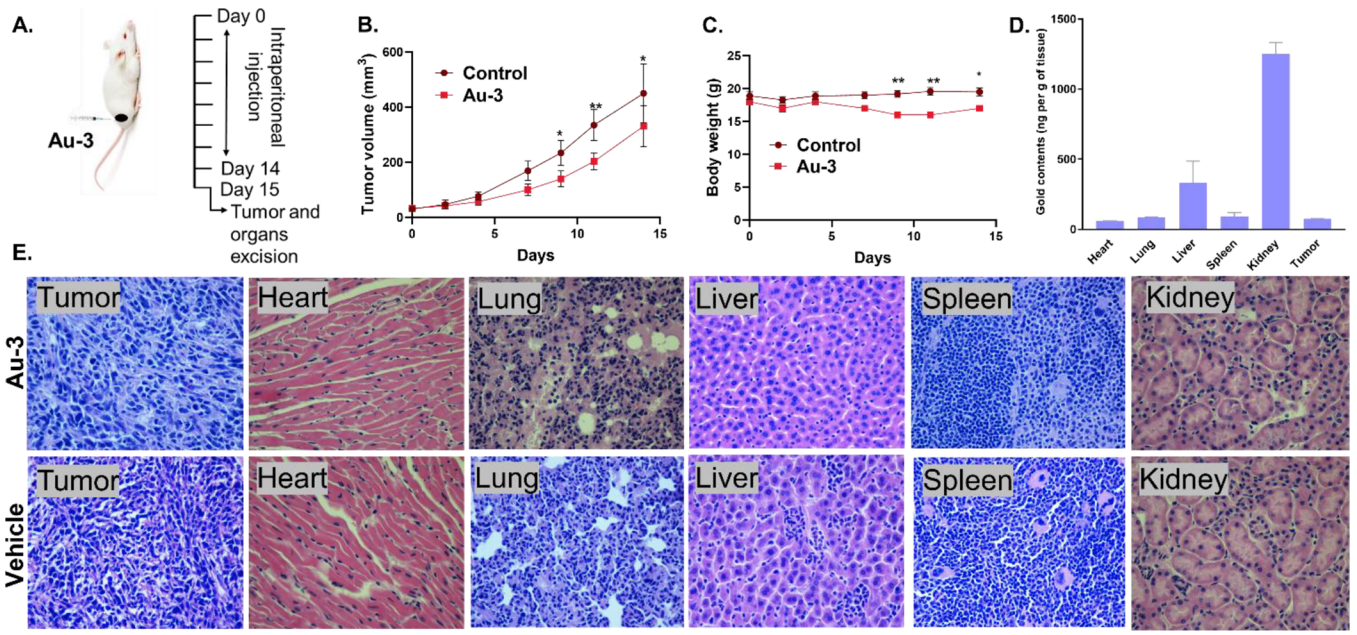

Figure 5. Therapeutic potential of **Au-3**. (A) Schematic diagram showing **Au-3** dosing schedule. (B,C) Effect of **Au-3** on tumor volume and weight of 4T1 infected Balb/c mice. Unpaired t test, *p < 0.05, **p < 0.01. (D) Histology (H&E) staining of harvested tissue and tumor. (E) Tissue biodistribution of **Au-3** determined by GF-AAS (n = 3).

with conjugated phosphanyl side groups and backbone (Figures 4B and S34−S59).

We further evaluated SAR by measuring the intracellular accumulation of **Au-1**−**Au-5** in cancer cell lines. MDA-MB-468 cells were treated with **Au-1**−**Au-5** at 10 μM for 18 h, and the intracellular accumulation of the compounds was determined by GF-AAS (Figure 4C). Cellular uptake of all compounds was above 400 pmol per million cells except **Au-5** that displayed low intracellular accumulation. This was attributed to the increased conjugated binaphthyl phosphanyl

https://doi.org/10.1021/acs.jmedchem.3c00238
J. Med. Chem. 2023, 66, 7868−7879

backbone of **Au-5** and limited solubility due to high lipophilicity. This result can further explain the higher IC_{50} values measured for **Au-5** in the four cancer cell lines tested compared to **Au-1**−**Au-4** (Table 1). Also, **Au-3** with an aliphatic ethane backbone showed the highest cellular uptake and corresponding low IC_{50} values, indicating that conjugation adversely impacts cellular uptake. To test the impact of the different phosphanyl groups on oxygen consumption rates and mitochondria membrane potential in isolated mitochondria from C57BL/6J mice, **Au-1**−**Au-3** was chosen, and we observed a concentration-dependent increase in OCR up to 8.3 μM with corresponding decrease in MMP. At a low concentration of 2.7 μM, **Au-3** displayed similar OCR levels comparable to **Au-1** and **Au-2** at a higher concentration of 8.3 μM showing that a low dose of **Au-3** is needed to induce uncoupling effect compared to **Au-1** or **Au-2** (Figure 4D−F). Taken together, these results validate the influence of the phosphanyl backbone and/or side groups on biological activity imposed by this class of compounds.

In Vivo Anticancer Activity. To illustrate the therapeutic impact on aggressive tumors, we assessed the efficacy of **Au-3** in vivo using a metastatic TNBC syngeneic model. Balb/c mice were injected with 4T1 murine TNBC cells subcutaneously (Figure 5A). The mice were administered intraperitoneally with **Au-3** at a dose of 10 mg/kg on alternate days, three times each week. Comparisons were made between the treatment group and a control group that received the vehicle (PBS solution containing 1% DMSO and 10% Kolliphor). We observed a significant tumor growth delay in 4T1 tumors; tumor growth inhibition measured at the end of the study was 36% (Figure 5B).

To assess preliminary toxicity of **Au-3**, we used body weight (Figure 5C). By the end of the study, mice did not lose >5% of body weight, suggestive of optimal tolerability. Biodistribution studies show significant accumulation in the kidney and liver, which suggest that these organs may be the major clearance hubs of Au-3 (Figure 5D). Furthermore, histological assessment to evaluate potential adverse effects by hematoxylin and eosin staining showed no signs of toxicity across all tissues examined (Figure 5E).

CONCLUSIONS

In summary, we show that [C^C]-cyclometalated Au(III), **Au-3**, exhibits mitochondrial uncoupling and impressive potency against aggressive cancer cells. Moreover, **Au-3** displays significant stability in blood serum, which is of clinical relevance and resist reduction from biological nucleophiles. Strikingly, the organometallic complex, **Au-3**, inhibits metastatic TNBC tumor growth in mice. Presumably, this report is likely the first account of a gold-based organometallic complex with mitochondrial uncoupling and promising antitumor activity. Our study fortifies the therapeutic value of organometallic gold agents and specifically provides the framework for the development of safe metal-based uncouplers.

EXPERIMENTAL PROCEDURES

General Information. Solvents used in this work were purchased from Pharmco-Aaper (ACS grade), and they were used as purchased. $HAuCl_4{\bullet}3H_2O$ was purchased from Nano Partz and stored under a nitrogen atmosphere. *S,S*-QuinoxP* was purchased from Strem Chemicals. 2,2-Dibromobiphenyl was purchased from Matrix scientific. (±)-2,2′-Bis(diphenylphosphino)-1,1′-binaphthalene was purchased from Oakwood chemicals. 1,2-Bis(diphenylphosphino)-ethane and di-*n*-butyl tin dichloride was purchased from Alfa Aesar. 1,2-Bis(diphenylphosphino)benzene was purchased from ChemScene. *N*-BuLi and anhydrous ether were purchased from Sigma Aldrich. 3-(4,5-Dimethylthiazol-2-yl)-2,5-diphenyltetrazolium bromide (MTT) was purchased from Cayman Chemicals. μ-Chloro biphenyl Au(III)[33,35,60] and 2,3-bis(diphenylphosphino)quinoxaline[37] were synthesized according to the reported procedures. Deuterated solvents were purchased from Cambridge Isotope Laboratories (Andover, MA). NMR spectra were recorded on a Bruker Avance NEO 400 MHz spectrometer and 500 MHz JEOL ECZr. Samples were calibrated for ^{1}H NMR ($CDCl_3$ δ = 7.26 ppm), ^{13}C(^{1}H-decoupled) NMR ($CDCl_3$ δ = 77.16), and ^{31}P(^{1}H-decoupled) NMR externally referenced to H_3PO_4 (δ = 0.00). High-resolution mass spectra (HRMS) were obtained by direct flow injection (injection volume = 2 μL) using ElectroSpray Ionization (ESI) on a Waters Synapt G2 HDMS instrument in the positive mode with a quadrupole/TOF analyzer (UC Boulder). Elemental analysis results were obtained from Atlantic Microlabs, Inc. (Norcross, GA). In addition to spectroscopic characterization, the purity of all compounds was assessed by RP-HPLC using an Agilent Technologies 1100 series HPLC instrument and an Agilent Phase Eclipse Plus C18 column (4.6 mm × 100 mm; 3.5 μm particle size). All compounds were found to be >97% pure. Fluorescent images were obtained from a fluorescence microscope in total internal reflection fluorescence (TIRF) and epifluorescence mode using 488 and 510 nm laser excitation, power 1 mW/cm^2 exposure time of 200 milliseconds using a 20× air objective. Images were processed with ImageJ software.

Synthesis and Characterization. *General Procedure for the Preparation of [Au-C^C-P^P] Compounds.* In a 50 mL round-bottom flask with a stir bar was added 7 mL of chloroform and μ-chloro biphenyl Au(III) (1.0 equiv). The corresponding bisphosphine ligand (1.0 equiv) was added. The solution was stirred at room temperature and monitored with TLC to show the completion of the reaction. The reaction was then purified on combiflash using 10% MeOH/DCM, precipitated from diethyl ether to afford the desired solid products.

Synthesis of Au-1. Prepared as described in the general procedure. μ-Chloro biphenyl Au(III) (30 mg, 0.039 mmol) and S,S-Quinox P* (13.04 mg, 0.039 mmol). Yield: 8.5 mg, 32% ^{1}H NMR (400 MHz, $CDCl_3$) δ (ppm) 8.44 (dd, 4 Hz, 2H), 8.17 (dd, 8 Hz, 2H), 7.83−7.88 (m, 2H), 7.55−7.57 (dq, 2H), 7.32 (t, 8 Hz, 2H), 7.19 (t, 8 Hz, 2H), 2.70 (d, 8 Hz, 6H), 1.22 (d, 16 Hz, 18H). ^{13}C NMR (101 MHz, $CDCl_3$): δ (ppm) 155.60, 155.59, 155.58, 153.34, 152.83, 143.68, 143.65, 143.61, 137.59, 137.52, 137.45, 135.32, 130.72, 129.43, 129.01, 128.87, 123.46, 123.44, 123.41, 37.36, 37.25, 37.14, 28.35, 28.33, 28.31, 6.20, 6.09, 6.06, 5.95. ^{31}P NMR (161.9 MHz, $CDCl_3$): δ (ppm) 44.34 APCI-MS (found) = 682.6 $[M-Cl]^+$ (calculated) = 683.2 Anal. Calcd: $C_{30}H_{36}AuClN_2P_2$: C, 50.12%; H, 5.05% Found: $C_{30}H_{36}AuClN_2P_2 \cdot 0.5\ C_4H_{10}O$: C, 50.81% H, 5.48%. Purity was determined to be >97% by RP-HPLC: R_f = 10.6 min using the following method: Flow rate: 1 mL/min; λ = 280 nm; Eluent A = DI water with 0.1% trifluoroacetic acid; Eluent B = Acetonitrile with 0.05% formic acid; Solvent Gradient: 0−16 min (0:100 H_2O:ACN). 16 min until end of run (100:0 H_2O:ACN).

Synthesis of Au-2. Prepared as described in the general procedure. μ-Chloro biphenyl Au(III) (40 mg, 0.05 mmol) and 1,2-Bis-(diphenylphosphino)benzene (23.22 mg, 0.05 mmol). Yield: 20 mg, 47% 1H NMR (500 MHz, $CDCl_3$): δ (ppm) 7.87 (dd, 10 Hz 2H), 7.63 (dd, 15 Hz, 8H), 7.50−7.56 (m, 8H), 7.39−7.43 (m, 8H), 7.05−7.16 (m, 4H), 6.58 (t, 10 Hz, 2H) ^{13}C NMR (125.7 MHz) δ (ppm) 121.01, 122.88, 122.93, 124.39, 124.90, 124.91, 126.79, 127.10, 128.14, 128.21, 128.27, 128.60, 130.18, 130.24, 130.30, 133.31, 133.58, 133.65, 134.86, 134.92, 134.98, 135.18, 135.22, 135.26, 136.00, 136.07, 136.15, 136.27, 136.34, 136.42, 137.91, 137.97, 138.18, 138.49, 138.64138.76, 154.98, 155.01, 162.03, 162.10, 163.18, 163.25 ^{31}PNMR (202.4 MHz) δ (ppm) 51.65 APCI-MS (found) = 794.5 $[M-Cl]^+$ (calculated) = 795.16. Anal. Calcd: $C_{42}H_{32}AuClP_2$ C, 60.7%, H, 3.88% Found: $C_{42}H_{32}AuClP_2 \cdot 0.65\ CH_2Cl_2$ C, 57.73% H 3.69%. Purity was determined to be >97% by RP-HPLC: R_f = 9.77 min using the following method: Flow rate: 1 mL/min; λ = 280 nm;

https://doi.org/10.1021/acs.jmedchem.3c00238
J. Med. Chem. 2023, 66, 7868−7879

Eluent A = DI water with 0.1% trifluoroacetic acid; Eluent B = Acetonitrile with 0.05% formic acid; Solvent Gradient: 0−16 min (0:100 H_2O:ACN). 16 min until end of run (100:0 H_2O:ACN).

Synthesis of Au-3. Prepared as described in the general procedure. μ-Chloro biphenyl Au(III) (60 mg, 0.078 mmol) and 1,2-bis(diphenylphosphino)ethane (31.08 mg, 0.078 mmol). Yield: 21 mg, 34.4%. ^{1}H NMR (500 MHz, $CDCl_3$): δ 7.82 (dd, 15, 10 Hz, 8H), 7.63 (t, 5 Hz, 4H), 7.56 (t, 5 Hz, 8H), 7.51 (t, 5 Hz, 2H), 7.12 (q, 10 Hz, 4H, 6.62 (t, 10 Hz, 2H), 3.31−3.42 (m, 4H), 13C NMR (125.7 MHz) δ 29.71, 30.0, 122.39, 122.45, 122.77, 123.28, 128.41, 128.70, 130.23, 130.35, 133.52, 134.17, 134.29, 137.40, 137.54, 155.05, 161.68, 161.74, 162.80, 162.87 ^{31}PNMR (202.4 MHz) δ 60.39 APCI-MS (found) = 746.5 $[M-Cl]^+$ (calculated) = 747.16 Anal. Calcd: $C_{38}H_{32}AuClP_2$: C, 58.29%; H, 4.12% Found: C, 57.16%, H, 4.2% $C_{38}H_{32}AuClP_2{\cdot}0.85H_2O$ Purity was determined to be >97% by RP-HPLC: R_f = 10.3 min using the following method: Flow rate: 1 mL/min; λ = 280 nm; Eluent A = DI water with 0.1% trifluoroacetic acid; Eluent B = Acetonitrile with 0.05% formic acid; Solvent Gradient: 0−16 min (0:100 H_2O:ACN). 16 min until end of run (100:0 H_2O:ACN).

Synthesis of Au-4. Prepared as described in the general procedure. μ-Chloro biphenyl Au(III), (40 mg, 0.05 mmol and 1,2-bis-(diphenylphosphino)quinoxaline (24.95 mg, 0.05 mmol). Yield: 27 mg, 58.7% ^{1}H NMR (500 MHz, $CDCl_3$): δ 8.11 (dd 10, 5 Hz 2H), 7.85−7.90 (m, 10H), 7.49 (d, 5 Hz, 2H), 7.44 (t, 10 Hz, 4H), 7.33 (t, 5 Hz, 7H), 7.19 (m, 2H), 7.10 (t, 10 Hz, 2 H), 6.97 (t, 5 Hz, 0.5H), 6.74 (t, 10 Hz, 0.5H), 6.57 (t, 5H, 2H). ^{13}C NMR (125 MHz, $CDCl_3$) 120.43, 122.28, 122.31, 122.33, 123.33,123.41, 123.66, 123.68, 123.93, 124.01, 126.25, 126.49, 127.49, 127.56, 127.63, 127.83, 129.02, 129.21, 129.27, 129.32, 129.50, 130.21, 132.52, 133.04, 133.20, 135.50, 135.56, 135.61, 136.10, 136.18, 136.26, 142.79, 142.83, 152.21, 154.53, 154.92, 155.51, 156.02, 156.10, 160.54, 161.61 ^{31}P NMR (202.4 MHz, $CDCl_3$) δ (ppm) 33.98 APCI-MS (found) = 846.5 $[M-Cl]^+$ (calculated) = 847.17 Elemental Analysis Anal. Calcd: $C_{44}H_{32}AuClN_2P_2$ C, 59.84%; H, 3.65%; Found: $C_{44}H_{32}AuClN_2P_2{\cdot}1.85H_2O{\cdot}0.1C_4H_{10}O$; C, 57.7% H, 3.99% Purity was determined to be >97% by RP-HPLC: R_f = 10.77 min using the following method: Flow rate: 1 mL/min; λ = 280 nm; Eluent A = DI water with 0.1% trifluoroacetic acid; Eluent B = Acetonitrile with 0.05% formic acid; Solvent Gradient: 0−16 min (0:100 H_2O:ACN). 16 min until end of run (100:0 H_2O:ACN).

Synthesis of Au-5. Prepared as described in the general procedure. μ-Chloro biphenyl Au(III), (40 mg, 0.05 mmol and (±)-2,2′-Bis(diphenylphosphino)-1,1′-binaphthalene (32.3 mg, 0.05 mmol). Yield: 18 mg, 34.3% ^{1}H NMR (500 MHz, $CDCl_3$): δ 8.26 (d, 5 Hz, 2H), 7.75−7.82 (m, 3H), 7.59 (d, 10 Hz, 4H), 7.53 (t, 5 Hz, 2H), 7.43 (t, 10 Hz, 6H), 7.37 (d, 10 Hz, 2H), 7.21 (d, 5 Hz, 4H), 7.15 (t, 10 Hz, 2H), 6.97−7.02 (m, 6H), 6.82 (t, 5 Hz, 2H), 6.70 (d, 10 Hz, 2H), 6.50 (q, 10 Hz, 2H), 6.33 (t, 10 Hz, 2H) ^{13}CNMR (175 MHz, $CDCl_3$) δ 156.02, 154.38, 152.31, 140.02, 139.95, 139.91, 136.45, 136.38, 136.31, 135.62, 135.52, 134.68, 134.61, 134.39, 134.31, 134.09, 133.28, 133.24, 133.03, 132.98, 132.85, 132.84, 132.78, 131.81, 130.61, 130.58130.55, 130.50, 129.23, 129.16, 128.81, 128.75, 128.69, 128.50, 128.40, 128.31, 128.11, 128.08, 128.05, 128.01, 127.91, 127.69, 127.57, 127.49, 127.44, 127.35, 126.52, 126.50, 126.30, 125.80, 124.75, 122.39, 122.37, 120.42, 119.25, 119.17 ^{31}P NMR (202.4 MHz) δ (ppm) 35.46 APCI-MS (found) = 970.4 $[M-Cl]^+$ (calculated) = 971.23 Elemental Analysis Anal. Calcd: $C_{56}H_{40}AuClP_2$ C, 66.77% H, 4.0% Found: $C_{56}H_{40}AuClP_2$ $C_{56}H_{40}AuClP_2{\cdot}1.35\ CH_2Cl_2$ C, 61.49% H, 3.66% Purity was determined to be >97% by RP-HPLC: R_f = 11.56 min using the following method: Flow rate: 1 mL/min; λ = 280 nm; Eluent A = DI water with 0.1% trifluoroacetic acid; Eluent B = Acetonitrile with 0.05% formic acid; Solvent Gradient: 0−16 min (0:100 H_2O:ACN). 16 min until end of run (100:0 H_2O:ACN).

Physical and Chemical Characterization. *X-ray Crystallography.* Diethylether was slowly diffused into concentrated solutions of **Au-1**, **Au-2a**, and **Au-3a** in dichloromethane at room temperature while **Au-2** was grown in slow diffusion of Et_2O into a concentrated solution of $CDCl_3$. Solid crystals were carefully examined under a microscope and mounted using polyisobutene oil on the end of a glass fiber, which had been mounted to a copper pin using an electrical solder. It was placed directly in the cold gas stream of a liquid nitrogen cryostat.[68,69] A Bruker D8 Venture diffractometer with graded multilayer focused MoKα X-rays (λ = 0.71073 Å) was used to collect diffraction. Raw data were integrated, scaled, merged, and corrected for Lorentz-polarization effects using the APEX3 package.[70−72] Space group determination and structure solution and refinement were carried out with SHELXT and SHELXL, respectively.[73,74] All non-hydrogen atoms were refined with anisotropic displacement parameters. Hydrogen atoms were placed at calculated positions and refined using a riding model with their isotropic displacement parameters (Uiso) set to either 1.2Uiso or 1.5Uiso of the atom to which they were attached. Ellipsoid plots were drawn using SHELXTL-XP.[75] The structures, deposited in the Cambridge Structural Database, were checked for missed symmetry, twinning, and overall quality with PLATON,[76] an R-tensor,[77] and finally validated using CheckCIF.[76]

Cyclic Voltammetry of Au-2 and Au-3. Electrochemical measurements of the ligands were recorded with a scan rate of 0.1 V/s with a three-segment sweep and a sample interval of 0.001 V. For complexes **Au-2** and **Au-3**, further characterization was performed by scanning at different rates (0.05, 0.1, 0.2, and 0.3 V/s). The quiet time was set to 2 s and sensitivity 1×10^{-4} A/V. All solutions were freshly prepared prior to use. All spectra were recorded using a CH instruments 650E potentiostat. The electrodes used were all 3 mm: a glassy carbon working electrode (CHI104), a Ag/AgCl reference electrode (CHI111), and a platinum wire counter electrode (CHI115). Both compounds **Au-2** and **Au-3** as well as both free ligands were prepared as a 5 mM solution in dry MeCN with NBu_4PF_6 (0.1 M) as the supporting electrolyte. The samples were purged with nitrogen for 30 min and recorded. Data were analyzed with GraphPad Prism 9.5.

Reactivity with GSH (UV−Vis Spectroscopy). Stock solutions of the complexes were prepared by dissolving an appropriate amount of compound and making a 1 mM solution in DMSO. The stock solutions were diluted down to 100 μM with DI H_2O. A separate stock solution of GSH was prepared as a 1 mM stock × 5 mL. All spectra were recorded on a Shimadzu UV-1280 model instrument. Prior to each recording, the instrument was blanked. The 1:10 solutions of the complex (100 μM) and GSH (1000 μM) were mixed, and the UV−vis spectra were recorded at the indicated time intervals. For each reaction, the spectrum was normalized to the highest absorbance and plotted in GraphPad Prism 9.5.

Reactivity with GSH (APCI−MS Analysis). Stock solutions of the complexes were prepared by dissolving an appropriate amount of compound and making a 1 mM stock solution in acetonitrile, and the solution was diluted to 100 μM. A separate stock solution of GSH was prepared as a 10 mM stock and diluted to 100 μM. A 1:1 solution of the complex **Au-1**−**Au-5** (100 μM) and GSH (100 μM) was mixed, and the solution was then subjected to APCI-MS analysis using an Agilent 1200 HPLC with a direct flow injection with an HPLC auto sampler without a column, λ = 280 nm, (injection volume: 40 μL, flow rate: 0.2 mL/min). ESI positive mode was taken with a source temperature of 120 °C, desolvation temperature of 300 °C, Capillary V at 3.5 kV while Cone was set at 35. Results were taken at 0, 1, 4, and 8 h intervals. Data were plotted and analyzed using Mestrenova.

In Vitro Biological Characterization. *Cell Culture.* Cancer cell lines (MDA-MB-231, MDA-MB-468, 4T1, and BT-333) used in this study were purchased from ATCC. MDA-MB-231, MDA-MB-468, and BT-333 were grown in DMEM supplemented with 10% FBS, 1% amphotericin, and 1% penicillin/streptomycin in a humidified incubator at 37 °C with 5−10% CO_2. The 4T1 cells were grown in RPMI supplemented with 10% FBS, 1% amphotericin, and 1% penicillin/streptomycin, and 4 mM glutamine.

Cell Viability of Complexes. The cytotoxicity assay of **Au-1**−**Au-5** and **cisplatin** was performed using 3-(4,5-dimethylthiazol-2-yl)-2,5-diphenyltetrazolium bromide assay (MTT assay) in MDA-MB-231, MDA-MB-468, BT-333, and 4T1 cancer cells. After the cells had reached confluency, Trypsin was added to detach and harvest the cells. The cells were washed in PBS and suspended in 10 mL of

https://doi.org/10.1021/acs.jmedchem.3c00238
J. Med. Chem. 2023, 66, 7868−7879

DMEM (or RPMI for 4T1 cells). The cells were centrifuged at 2000 rpm for 5 min, media decanted, and resuspended in 5 mL of the appropriate medium. The cells were plated in a 96-well clear bottom plate at a density of 4000 cells per well and left to adhere overnight at 37 °C with 5−10% CO_2. **Au-1**−**Au-5** and cisplatin were prepared as a stock in DMSO and PBS, respectively, and added at seven different concentrations starting at 100 μM for the highest concentration with a 3× serial dilution for subsequent wells and incubated at 37 °C for 72 h with 5−10% CO_2. After 72 h, the media was removed and replaced with a solution of MTT (100 μL, prepared by dissolving MTT at 5 mg/mL and diluting by 10× with DMEM) was added to each well and incubated for 4 h at 37 °C with 5−10% CO_2. The dye was removed from each well, and 100 μL of DMSO was added to induce cell lysis. The plates were read using a Genios plate reader (λ = 570 nm). The experiment was performed in triplicate, and data are plotted as the mean ± SEM (n = 3). Data can be found in the main text and the other complexes can be seen in the supplementary figures.

Whole Cell Uptake Analysis. MDA-MB-468 cells (1×10^6) were seeded in a 6-well plate and allowed to adhere overnight at 37 °C. Cells were treated with compound for 18 h, collected via trypsinization, and centrifuged at 2000 rpm for 5 min to form a pellet. The pellet was suspended in 1 mL of DMEM, transferred to 1.5 mL Eppendorf tube, and centrifuged at 2000 rpm for 5 min. The media was removed, and pellets were resuspended and washed in PBS (1 mL × 2) and stored at −20 °C until further analysis. Prior to analysis, pellets were suspended in 70% HNO_3 200 μL, digested for 4 h, allowed to cool to room temperature, and diluted appropriately before being analyzed on GF-AAS. Cellular gold concentration was expressed as pmol of Au per million cells.

Apoptosis Analysis. MDA-MB-231 cells were seeded at a density of 5×10^5 cells/well in a 6-well clear bottom plate with a final media volume of 2 mL. The cells were allowed to adhere overnight at 37 °C. A stock of **Au-3** was prepared fresh in DMSO and added to the desired well at a concentration of 1 μM with a final volume of 2.5 mL and incubated for 4 h at 37 °C. A stock of H_2O_2 was prepared in PBS and the cells were treated at a final concentration of 2 mM for 1 h as a positive control. When ready for analysis, the media were removed, and the wells were washed with 5 mL of PBS. The cells were trypsinized (1 mL), 5 mL of DMEM was added to each well, and the total volume was collected and centrifuged to pellet the cells. The cells were resuspended in 2 mL of fresh media, counted, and reconstituted to a concentration of 1×10^5 cells/mL. The cells were centrifuged again, and the pellets were suspended in 500 μL of Annexin binding buffer. To each sample was added 5 μL of Annexin V-FITC and 5 μL PI and incubated in the dark at room temperature for 5 min. The samples were then subjected to FACS analysis. Graphs are representative of three technical replicates.

MDA-MB-468 Mitochondria Respiration Analysis. MDA-MB-468 cells (30,000 cells per well) were seeded in an XF96 Seahorse plate and allowed to adhere overnight in an incubator at 37 °C with 5−10% CO_2. **Au-3** and cisplatin were prepared as stock solution in DMSO and PBS, respectively, and diluted to 75 μM with Seahorse XF96 assay buffer and then subsequently serial-diluted by 3× to achieve multiple concentrations and added for 12 h prior to measurement on the XF96 Seahorse. This was followed by injection of oligomycin (1.5 μM), FCCP (0.6 μM), and rotenone/antimycin A (0.5 μM). The metabolic parameters were calculated from the reading obtained from a minimum of 6 wells.

Cell Cycle Analysis. MDA-MB-468 cells were seeded at a density of 2×10^5 cells/well in a 6-well clear bottom plate with a final media volume of 2 mL and allowed to adhere overnight 37 °C. **Au-3** was prepared fresh as a stock in DMSO and added at a concentration of 0.5 and 1 μM with a final volume of 2.5 mL for 12 h. After 12 h, the medium was removed and added to a 15 mL Falcon tube. The wells were washed with PBS (5 mL), trypsinized (1 mL), and 5 mL of fresh DMEM was added. All media were combined, and the tube was centrifuged at 2000 rpm for 5 min to collect the pellet. The pellet was resuspended in 1 mL of PBS, transferred to a 1 mL Eppendorf tube, centrifuged at 2000 rpm for 5 min, decanted, and resuspended in 70% EtOH/PBS solution. This solution was stored at 4 °C until ready for analysis. Prior to analysis, the stored cells were collected by centrifuging at 2000 rpm for 5 min, washed twice with PBS (1 mL), and resuspended in 50 μL of RNase solution (100 mg/mL) and 200 μL of 50 mg/mL PI solution. The solutions were then filtered through a 5 mL round polystyrene bottom tube fit with a cell-strainer cap. The samples were then analyzed with FACS. Data are representative of three technical replicates with percentages plotted as the mean ± SEM (n = 3).

■ ANIMAL EXPERIMENT

Mouse Liver Mitochondrial Membrane Potential. The differential mitochondrial isolation method was used to isolate mouse liver. Mitochondria were isolated from 8−9-week-old mice. Ten micrograms of mito were run on an HTX plate reader containing 100 μL of respiration buffer. The membrane potential was monitored using TMRE dye (150 nM final concentration). Compounds **Au-3** was dissolved in DMSO to make 25 mM stock solutions. The stocks were further diluted 1:10 in DMSO to prepare working stock 2.5 mM. The working stock was serially diluted (5 times) 1:3 in DMSO to prepare further dilutions 0.83, 0.27, 0.09, 0.03 and 0.01 mM. One microliter of each of these dilutions was added to the reaction well containing respiration buffer to have final concentrations of the compound as 25, 8.3, 2.7, 0.9, 0.3, and 0.1 μM, respectively. Results for 25 and 8.3 μM are not included. The plate was read at λ = 530ex/590em with the mito and subsequently after the addition of pyruvate + malate, oligomycin, and FCCP. The difference (Δ) between FCCP−oligomycin was taken as a maximum membrane potential difference between the coupled and uncoupled states of respiration.

Mouse Liver Mitochondria Respiration Using Seahorse. Mouse Liver mitochondria isolated from 8 to 9-week-old C57BL/6 mouse using differential mito isolation was used for this study. Five micrograms of mito per well were run on Seahorse (XFe96) containing respiration buffer. Compounds **Au-3** were dissolved in DMSO to make 25 mM stock solutions. The stocks were further diluted 1:10 in DMSO to prepare stock of 2.5 mM. The working stock was serially diluted (5 times) 1:3 in DMSO to prepare further dilutions (each of 100×) 0.83, 0.27, 0.09, 0.03, and 0.01 mM. Sixteen microliters of each of these dilutions (100×) were added to 186 μL of respiration buffer, and 25 μL was added to the reaction well containing respiration buffer to have final concentrations of the compound as 25 μm, 8.3 μM, 2.7 μM, 0.9 μM, 0.3 μM, and 0.1 μM, respectively. The oxygen consumption rates (OCR) were monitored after compound addition during top up volume (25 μL) followed by pyruvate + malate + ADP, oligomycin, FCCP, and rotenone+succinate addition through injection ports A, B, C, and D, respectively, and measuring OCR after each addition.

In Vivo Experiment. Five-week-old female BALB/c mice were purchased from Jackson Laboratories and quarantined for a period of one week before inoculation with 1,000,000 4T1 cells subcutaneously on their right flanks. After 3 days of implantation, the mice were systemically treated with 10 mg/kg **Au-3** via intraperitoneal administration. **Au-3** was formulated in DMSO (1%), Kolliphor (10%), and PBS (89%) and delivered at 100 μL. The control group was treated with a PBS solution containing 1% DMSO and 10% Kolliphor. The injection of **Au-3** was performed three times a week for two weeks. Tumor size and body weight measurements were performed three days a week, and mice were

https://doi.org/10.1021/acs.jmedchem.3c00238
J. Med. Chem. 2023, 66, 7868−7879

euthanized 15 days later. All mice were maintained in a pathogen-free environment under the care of DLAR of University of Kentucky. Our study was performed in compliance with the NIH guidelines (NIH Publication No. 85-23 Rev. 1985) for the care and use of laboratory animals and all experimental procedures were monitored and approved by the Institutional Animal Care and Use Committee (IACUC) of University of Kentucky (USA).

Hematoxylin and Eosin Staining. The mice used in the in vivo comparative experiment of **Au-3** were sacrificed at day 14 post tumor cell (4T1) injection. Freshly prepared paraformaldehyde (4% in PBS) was used to fix harvested mice organs (heart, lung, liver, kidney, spleen, and tumor) for 24 h before being processed for paraffin sectioning. The organ sections of 5 μm were stained with H&E staining and used for histological examination of the organs and tumor. A total of 5 sections per tissue (spanning the full depth of the organ) were examined and photographed using a Nikon Eclipse 55i microscope.

Tissue Biodistribution. Tissues obtained from the in vivo studies were used for tissue biodistribution. The tissues were boiled for 5 h at 60 °C with 70% HNO_3 (0.5 mL) and then boiled again at 60 °C for 10 min by adding 35% hydrogen peroxide (0.5 mL). The solution turned yellow and was diluted as needed to measure the gold content using a Graphite Furnace Atomic Absorption Spectrometer. Before measuring all samples, the standard solution curves were measured.

Serum Stability. Blood samples were taken from 14 weeks old BALB/cJ female mice and used for serum stability. Au-3 was prepared as a 100 mM stock solution in DMSO. Au-3 (2.5 μL) was taken and mixed with 247.5 μL of serum to make a final volume of 250 μL. For the experiment, serum containing Au-3 (17 μL) was mixed with MeOH (80 μL). The solution was vortexed for 1 min and centrifuged at 14,000 rpm at 4 °C for 10 min. The clear supernatants were taken and subjected to LC−MS analysis at different time points (0, 10, 30, 60, 120, 360, and 1440 min). The result was plotted as the % of Au-3 serum stability against time. All experiments were performed in duplicate.

■ ASSOCIATED CONTENT

Supporting Information

The Supporting Information is available free of charge at https://pubs.acs.org/doi/10.1021/acs.jmedchem.3c00238.

Crystal data and structure refinement for compounds **Au-1**, **Au-2**, **Au-2a**, **Au-3a**; ^{1}H, ^{13}C, ^{31}P spectra, HPLC traces, APCI-MS, electrochemistry, and UV−vis spectra for compounds **Au-1**−**Au-5**; dose response graphs for compounds **Au-1**−**Au-5** and cisplatin, apoptosis Au-3, standard curve for in vivo biodistribution of Au-3 (S69) mitochondria membrane potential of isolated mitochondria of C57BL/6J mice treated with **Au-1** and **Au-2** using TMRE dye; mitostress assay of cisplatin (S70); and whole cell uptake of **Au-1**−**Au-5** (PDF)

Molecular formular strings (CSV)

■ AUTHOR INFORMATION

Corresponding Author

Samuel G. Awuah − *Department of Chemistry, University of Kentucky, Lexington, Kentucky 40506, United States; Center for Pharmaceutical Research and Innovation and Department of Pharmaceutical Sciences, College of Pharmacy University of Kentucky, Lexington, Kentucky 40536, United States; Markey Cancer Center, University of Kentucky, Lexington, Kentucky 40536, United States;* orcid.org/0000-0003-4947-7283; Email: awuah@uky.edu

Authors

Adedamola S. Arojojoye − *Department of Chemistry, University of Kentucky, Lexington, Kentucky 40506, United States;* orcid.org/0000-0003-3076-264X

Chibuzor Olelewe − *Department of Chemistry, University of Kentucky, Lexington, Kentucky 40506, United States*

Sailajah Gukathasan − *Department of Chemistry, University of Kentucky, Lexington, Kentucky 40506, United States*

Jong H. Kim − *Department of Chemistry, University of Kentucky, Lexington, Kentucky 40506, United States*

Hemendra Vekaria − *Spinal Cord and Brain Injury Research Center and Department of Neuroscience, University of Kentucky, Lexington, Kentucky 40536, United States*

Sean Parkin − *Department of Chemistry, University of Kentucky, Lexington, Kentucky 40506, United States*

Patrick G. Sullivan − *Spinal Cord and Brain Injury Research Center, Department of Neuroscience, and Department of Neuroscience, University of Kentucky, Lexington, Kentucky 40536, United States;* orcid.org/0000-0001-7418-4760

Complete contact information is available at: https://pubs.acs.org/10.1021/acs.jmedchem.3c00238

Author Contributions

Conceptualization, A.S.A. and S.G.A.; methodology, A.S.A.; synthesis and characterization, A.S.A.; X-ray crystallography, S.R.P.; Biological assays, A.S.A. and C.O.; APCI-MS studies A.S.A. and S.G., Serum stability studies S.G. and J.H.K., In vivo studies, C.O. and J.H.K.; Seahorse assay and MMP studies A.S.A., H.V., P.G.S. and S.G.A. Electrochemistry, UV−vis spectrometry A.S.A., ; writing—original draft preparation, A.S.A. and S.G.A.; writing—review and editing, A.S.A. and S.G.A.; supervision, S.G.A.; funding acquisition, S.G.A.

Notes

The authors declare the following competing financial interest(s): The authors declare the following financial interests/personal relationships which may be considered as potential competing interests: Samuel G. Awuah has patents pending to University of Kentucky Research Foundation.

■ ACKNOWLEDGMENTS

We are grateful for financial support from the National Cancer Institute (NCI) R01CA258421-01 (S.G.A.). We would like to thank the following facilities at the University of Kentucky who provided support in completion of the experiments detailed in this manuscript. The UK NMR Center supported by NSF (CHE-997738) and the UK X-ray facility supported by the MRI program from NSF (CHE-1625732). For the flow cytometry experiments, we would like to thank UK Flow Cytometry and Immune Function core supported by the Office of the Vice President of Research, the Markey Cancer Center, and NCI Center Core Support Grant (P30 CA177558). We thank Dr. Chris Richard's lab for access and assistance with fluorescence microscopy. We would also like to thank Dr. Steven Van Lanen's laboratory for access to their APCI-MS.

https://doi.org/10.1021/acs.jmedchem.3c00238
J. Med. Chem. 2023, 66, 7868−7879

■ ABBREVIATIONS

APCI-MS, atmospheric pressure chemical ionization mass spectrometry; ATP, adenosine triphosphate; AUC, area under the curve; DMEM, Dulbecco's modified eagle medium; DNP, dinitrophenol; DPPE, 1,2-Bis(diphenylphosphino)ethane; ESI, electrospray ionization; FBS, fetal bovine serum; GF-AAS, graphite furnace atomic absorption spectrometry; HPLC, high performance liquid chromatography; L-GSH, L-glutathione; MMP, mitochondria membrane potential; NHC, N-heterocyclic carbene; ORTEP, oak ridge thermal ellipsoid plot; PBS, phosphate buffer saline; TMRE, tetramethylrhodamine, ethyl ester; TNBC, triple negative breast cancer

■ REFERENCES

(1) Siegel, R. L.; Miller, K. D.; Wagle, N. S.; Jemal, A. Cancer statistics, 2023. *CA Cancer J. Clin.* **2023**, *73*, 17−48.

(2) Chhikara, B. S.; Parang, K. Global Cancer Statistics 2022: the trends projection analysis. *Chem. Biol. Lett.* **2023**, *10*, 451−451.

(3) Schlichtig, K.; Dürr, P.; Dörje, F.; Fromm, M. F. New oral anticancer drugs and medication safety. *Dtsch. Arztebl. Int.* **2019**, *116*, 775.

(4) Williams, A. M.; Liu, Q.; Bhakta, N.; Krull, K. R.; Hudson, M. M.; Robison, L. L.; Yasui, Y. Rethinking success in pediatric oncology: beyond 5-year survival. *J. Clin. Oncol.* **2021**, *39*, 2227.

(5) Yeh, J. M.; Ward, Z. J.; Chaudhry, A.; Liu, Q.; Yasui, Y.; Armstrong, G. T.; Gibson, T. M.; Howell, R.; Hudson, M. M.; Krull, K. R.; Leisenring, W. M.; Oeffinger, K. C.; Diller, L. Life expectancy of adult survivors of childhood cancer over 3 decades. *JAMA Oncol.* **2020**, *6*, 350−357.

(6) Yue, S.; Luo, M.; Liu, H.; Wei, S. Recent advances of gold compounds in anticancer immunity. *Front. Chem.* **2020**, *8*, 543.

(7) Fernández-Moreira, V.; Herrera, R. P.; Gimeno, M. C. Anticancer properties of gold complexes with biologically relevant ligands. *Pure Appl. Chem.* **2019**, *91*, 247−269.

(8) Mertens, R. T.; Gukathasan, S.; Arojojoye, A. S.; Olelewe, C.; Awuah, S. G. Next Generation Gold Drugs and Probes: Chemistry and Biomedical Applications. *Chem. Rev.* **2023**, *123*, 6612.

(9) Yamashita, M. Auranofin: Past to Present, and repurposing. *Int. Immunopharmacol.* **2021**, *101*, 108272.

(10) Liu, Y.; Lu, Y.; Xu, Z.; Ma, X.; Chen, X.; Liu, W. Repurposing of the gold drug auranofin and a review of its derivatives as antibacterial therapeutics. *Drug Discovery Today* **2022**, *27*, 1961.

(11) Olelewe, C.; Kim, J. H.; Ofori, S.; Mertens, R. T.; Gukathasan, S.; Awuah, S. G. Gold (III)-P-chirogenic complex induce mitochondrial dysfunction in triple-negative breast cancer. *iScience* **2022**, *25*, No. 104340.

(12) Gukathasan, S.; Awuah, S. G. Synthetic Strategies for the Preparation of Gold-based Anticancer Agents. In *Encyclopedia of Inorganic and Bioinorganic Chemistry*; Scott, R. A., Ed.; 2022, 1-32, DOI: 10.1002/9781119951438.eibc2822.

(13) Bao, M.; Zhou, S.; Hu, W.; Xu, X. Recent advances in gold-complex and chiral organocatalyst cooperative catalysis for asymmetric alkyne functionalization. *Chin. Chem. Lett.* **2022**, *33*, 4969.

(14) Lu, Y.; Ma, X.; Chang, X.; Liang, Z.; Lv, L.; Shan, M.; Lu, Q.; Wen, Z.; Gust, R.; Liu, W. Recent development of gold (I) and gold (III) complexes as therapeutic agents for cancer diseases. *Chem. Soc. Rev.* **2022**, *51*, 5518.

(15) Mulks, F. F. Gold carbene complexes and beyond: new avenues in gold (I)-carbon coordination chemistry. *Gold Bull.* **2022**, *55*, 1−13.

(16) Arojojoye, A. S.; Mertens, R. T.; Ofori, S.; Parkin, S. R.; Awuah, S. G. Synthesis, Characterization, and Antiproliferative Activity of Novel Chiral [QuinoxP* AuCl2]+ Complexes. *Molecules* **2020**, *25*, 5735.

(17) Gurba, A.; Taciak, P.; Sacharczuk, M.; Młynarczuk-Biały, I.; Bujalska-Zadrożny, M.; Fichna, J. Gold (III) derivatives in colon cancer treatment. *Int. J. Mol. Sci.* **2022**, *23*, 724.

(18) Berners-Price, S. J.; Mirabelli, C. K.; Johnson, R. K.; Mattern, M. R.; McCabe, F. L.; Faucette, L. F.; Sung, C.-M.; Mong, S.-M.; Sadler, P. J.; Crooke, S. T. In vivo antitumor activity and in vitro cytotoxic properties of bis [1, 2-bis (diphenylphosphino) ethane] gold (I) chloride. *Cancer Res.* **1986**, *46*, 5486−5493.

(19) Hickey, J. L.; Ruhayel, R. A.; Barnard, P. J.; Baker, M. V.; Berners-Price, S. J.; Filipovska, A. Mitochondria-targeted chemotherapeutics: the rational design of gold (I) N-heterocyclic carbene complexes that are selectively toxic to cancer cells and target protein selenols in preference to thiols. *J. Am. Chem. Soc.* **2008**, *130*, 12570−12571.

(20) Nardon, C.; Schmitt, S. M.; Yang, H.; Zuo, J.; Fregona, D.; Dou, Q. P. Gold (III)-dithiocarbamato peptidomimetics in the forefront of the targeted anticancer therapy: Preclinical studies against human breast neoplasia. *PLoS One* **2014**, *9*, No. e84248.

(21) Chow, K. H.-M.; Sun, R. W.-Y.; Lam, J. B.; Li, C. K.-L.; Xu, A.; Ma, D.-L.; Abagyan, R.; Wang, Y.; Che, C.-M. A gold (III) porphyrin complex with antitumor properties targets the Wnt/β-catenin pathway. *Cancer Res.* **2010**, *70*, 329−337.

(22) Che, C.-M.; Sun, R. W.-Y.; Yu, W.-Y.; Ko, C.-B.; Zhu, N.; Sun, H. Gold (III) porphyrins as a new class of anticancer drugs: cytotoxicity, DNA binding and induction of apoptosis in human cervix epitheloid cancer cells. *Chem. Commun.* **2003**, 1718−1719.

(23) Sun, R. W.-Y.; Che, C.-M. The anti-cancer properties of gold (III) compounds with dianionic porphyrin and tetradentate ligands. *Coord. Chem. Rev.* **2009**, *253*, 1682−1691.

(24) Wang, Y.; He, Q. Y.; Che, C. M.; Chiu, J. F. Proteomic characterization of the cytotoxic mechanism of gold (III) porphyrin 1a, a potential anticancer drug. *Proteomics* **2006**, *6*, 131−142.

(25) Zou, T.; Lum, C. T.; Lok, C.-N.; Zhang, J.-J.; Che, C.-M. Chemical biology of anticancer gold (III) and gold (I) complexes. *Chem. Soc. Rev.* **2015**, *44*, 8786−8801.

(26) Oberkofler, J.; Aikman, B.; Bonsignore, R.; Pöthig, A.; Platts, J.; Casini, A.; Kühn, F. E. Exploring the Reactivity and Biological Effects of Heteroleptic N-Heterocyclic Carbene Gold (I)-Alkynyl Complexes. *Eur. J. Inorg. Chem.* **2020**, *2020*, 1040−1051.

(27) Di Sarra, F.; Fresch, B.; Bini, R.; Saielli, G.; Bagno, A. Reactivity of auranofin with selenols and thiols−implications for the anticancer activity of gold (I) compounds. *Eur. J. Inorg. Chem.* **2013**, *2013*, 2718−2727.

(28) Yangyuoru, P. M.; Webb, J. W.; Shaw, C. F., III Glutathionato-S-Gold (III) complexes formed as intermediates in the reduction of auricyanide by glutathione. *J. Inorg. Biochem.* **2008**, *102*, 584−593.

(29) Đurović, M. D.; Bugarčić, Z. D.; Heinemann, F. W.; van Eldik, R. Substitution versus redox reactions of gold (III) complexes with L-cysteine, L-methionine and glutathione. *Dalton Trans.* **2014**, *43*, 3911−3921.

(30) Arojojoye, A. S.; Kim, J. H.; Olelewe, C.; Parkin, S.; Awuah, S. G. Chiral gold (III) complexes: speciation, in vitro, and in vivo anticancer profile. *Chem. Commun.* **2022**, *58*, 10237−10240.

(31) Nilakantan, L.; McMillin, D. R.; Sharp, P. R. Emissive biphenyl cyclometalated gold (III) diethyl dithiocarbamate complexes. *Organometallics* **2016**, *35*, 2339−2347.

(32) David, B.; Monkowius, U.; Rust, J.; Lehmann, C.; Hyzak, L.; Mohr, F. Gold (III) compounds containing a chelating, dicarbanionic ligand derived from 4, 4′-di-tert-butylbiphenyl. *Dalton Trans.* **2014**, *43*, 11059−11066.

(33) Usón, R.; Vicente, J.; Cirac, J.; Chicote, M. Synthesis and reactivity of dibenzometallole complexes of gold (III) and platinum (II). *J. Organomet. Chem.* **1980**, *198*, 105−112.

(34) Joost, M.; Estévez, L.; Miqueu, K.; Amgoune, A.; Bourissou, D. Oxidative addition of carbon−carbon bonds to gold. *Angew. Chem., Int. Ed.* **2015**, *127*, 5325−5329.

(35) Wu, C.-Y.; Horibe, T.; Jacobsen, C. B.; Toste, F. D. Stable gold(III) catalysts by oxidative addition of a carbon−carbon bond. *Nature* **2015**, *517*, 449−454.

(36) Khodjoyan, S.; Remadna, E.; Dossmann, H.; Lesage, D.; Gontard, G.; Forté, J.; Hoffmeister, H.; Basu, U.; Ott, I.; Spence, P.; Waller, Z. A. E.; Salmain, M.; Bertrand, B. [(C C) Au (N N)]+

https://doi.org/10.1021/acs.jmedchem.3c00238
J. Med. Chem. 2023, 66, 7868−7879

Complexes as a New Family of Anticancer Candidates: Synthesis, Characterization and Exploration of the Antiproliferative Properties. *Chem. – Eur. J.* **2021**, *27*, 15773−15785.
(37) Adam, M. S. S.; Mohamad, A. D.; Jones, P. G.; Kindermann, M. K.; Heinicke, J. W. Comparison of the reactivity of 2-amino-3-chloro- and 2, 3-dichloroquinoxalines towards Ph2PH and Ph2PLi and of the properties of diphenylphosphanyl-quinoxaline P, N and P, P ligands. *Polyhedron* **2013**, *50*, 101−111.
(38) Mirabell, C. K.; Johnson, R. K.; Hill, D. T.; Faucette, L. F.; Girard, G. R.; Kuo, G. Y.; Sung, C. M.; Crooke, S. T. Correlation of the in vitro cytotoxic and in vivo antitumor activities of gold (I) coordination complexes. *J. Med. Chem.* **1986**, *29*, 218−223.
(39) Mirabelli, C. K.; Hill, D. T.; Faucette, L. F.; McCabe, F. L.; Girard, G. R.; Bryan, D. B.; Sutton, B. M.; Barus, J. O. L.; Crooke, S. T.; Johnson, R. K. Antitumor activity of bis (diphenylphosphino) alkanes, their gold (I) coordination complexes, and related compounds. *J. Med. Chem.* **1987**, *30*, 2181−2190.
(40) Berners-Price, S. J.; Sadler, P. J. Gold (I) complexes with bidentate tertiary phosphine ligands: formation of annular vs. tetrahedral chelated complexes. *Inorg. Chem.* **1986**, *25*, 3822−3827.
(41) Berners-Price, S. J.; Girard, G. R.; Hill, D. T.; Sutton, B. M.; Jarrett, P. S.; Faucette, L. F.; Johnson, R. K.; Mirabelli, C. K.; Sadler, P. J. Cytotoxicity and antitumor activity of some tetrahedral bis (diphosphino) gold (I) chelates. *J. Med. Chem.* **1990**, *33*, 1386−1392.
(42) Carlos Lima, J.; Rodriguez, L. Phosphine-gold (I) compounds as anticancer agents: general description and mechanisms of action. *Anti-Cancer Agents Med. Chem.* **2011**, *11*, 921−928.
(43) Caruso, F.; Rossi, M.; Tanski, J.; Pettinari, C.; Marchetti, F. Antitumor activity of the mixed phosphine gold species chloro-triphenylphosphine-1, 3-bis (diphenylphosphino) propanegold (I). *J. Med. Chem.* **2003**, *46*, 1737−1742.
(44) Higginbotham, M. L.; Henry, C. J.; Katti, K. V.; Casteel, S. W.; Dowling, P. M.; Pillarsetty, N. Preclinical tolerance and pharmacokinetic assessment of MU-Gold, a novel chemotherapeutic agent, in laboratory dogs. *Vet. Ther.* **2003**, *4*, 76−82.
(45) Dennis, E. K.; Kim, J. H.; Parkin, S.; Awuah, S. G.; Garneau-Tsodikova, S. Distorted Gold (I)−Phosphine Complexes as Antifungal Agents. *J. Med. Chem.* **2020**, *63*, 2455−2469.
(46) Kim, J. H.; Reeder, E.; Parkin, S.; Awuah, S. G. Gold (I/III)-phosphine complexes as potent antiproliferative agents. *Sci. Rep.* **2019**, *9*, 12335.
(47) Olelewe, C.; Kim, J. H.; Ofori, S.; Mertens, R. T.; Gukathasan, S.; Awuah, S. G. Gold(III)-P-chirogenic complex induces mitochondrial dysfunction in triple-negative breast cancer. *iScience* **2022**, *25*, No. 104340.
(48) Keter, F. K.; Guzei, I. A.; Nell, M.; Zyl, W. E. V.; Darkwa, J. Phosphinogold (I) dithiocarbamate complexes: effect of the nature of phosphine ligand on anticancer properties. *Inorg. Chem.* **2014**, *53*, 2058−2067.
(49) Horvath, U. E.; Dobrzańska, L.; Strasser, C. E.; Bouwer, W.; Joone, G.; van Rensburg, C. E. J.; Cronje, S.; Raubenheimer, H. G. Amides of gold (I) diphosphines prepared from N-heterocyclic sources and their in vitro and in vivo screening for anticancer activity. *J. Inorg. Biochem.* **2012**, *111*, 80−90.
(50) Demine, S.; Renard, P.; Arnould, T. Mitochondrial uncoupling: a key controller of biological processes in physiology and diseases. *Cell* **2019**, *8*, 795.
(51) Kotova, E. A.; Antonenko, Y. N. Fifty years of research on protonophores: Mitochondrial uncoupling as a basis for therapeutic action. *Acta Nat.* **2022**, *14*, 4.
(52) Hirschenson, J.; Melgar-Bermudez, E.; Mailloux, R. J. The uncoupling proteins: a systematic review on the mechanism used in the prevention of oxidative stress. *Antioxidants* **2022**, *11*, 322.
(53) Ardalan, A.; Smith, M. D.; Jelokhani-Niaraki, M. Uncoupling Proteins and Regulated Proton Leak in Mitochondria. *Int. J. Mol. Sci.* **2022**, *23*, 1528.
(54) Goedeke, L.; Shulman, G. I. Therapeutic potential of mitochondrial uncouplers for the treatment of metabolic associated fatty liver disease and NASH. *Mol. Metabol.* **2021**, *46*, No. 101178.
(55) Shrestha, R.; Johnson, E.; Byrne, F. L. Exploring the therapeutic potential of mitochondrial uncouplers in cancer. *Mol. Metabol.* **2021**, *51*, No. 101222.
(56) Čater, M.; Bombek, L. K. Protective Role of Mitochondrial Uncoupling Proteins against Age-Related Oxidative Stress in Type 2 Diabetes Mellitus. *Antioxidants* **2022**, *11*, 1473.
(57) Bonanno, J. A.; Shyam, R.; Choi, M.; Ogando, D. G. The H+ transporter SLC4A11: Roles in metabolism, oxidative stress and mitochondrial uncoupling. *Cell* **2022**, *11*, 197.
(58) Hoke, G. D.; Rush, G.; Bossard, G.; McArdle, J.; Jensen, B. D.; Mirabelli, C. Mechanism of alterations in isolated rat liver mitochondrial function induced by gold complexes of bidentate phosphines. *J. Biol. Chem.* **1988**, *263*, 11203−11210.
(59) Hoke, G. D.; Macia, R. A.; Meunier, P. C.; Bugelski, P. J.; Mirabelli, C. K.; Rush, G. F.; Matthews, W. D. In vivo and in vitro cardiotoxicity of a gold-containing antineoplastic drug candidate in the rabbit. *Toxicol. Appl. Pharmacol.* **1989**, *100*, 293−306.
(60) Chan, K. T.; Tong, G. S. M.; Wan, Q.; Cheng, G.; Yang, C.; Che, C. M. Strongly Luminescent Cyclometalated Gold (III) Complexes Supported by Bidentate Ligands Displaying Intermolecular Interactions and Tunable Emission Energy. *Chem. – Asian J.* **2017**, *12*, 2104−2120.
(61) Babak, M. V.; Chong, K. R.; Rapta, P.; Zannikou, M.; Tang, H. M.; Reichert, L.; Chang, M. R.; Kushnarev, V.; Heffeter, P.; Meier-Menches, S. M.; Lim, Z. C.; Yap, J. Y.; Casini, A.; Ang, W. H. Interfering with Metabolic Profile of Triple-Negative Breast Cancers Using Rationally Designed Metformin Prodrugs. *Angew. Chem., Int. Ed.* **2021**, *60*, 13405−13413.
(62) Huang, K.-B.; Wang, F.-Y.; Tang, X.-M.; Feng, H.-W.; Chen, Z.-F.; Liu, Y.-C.; Liu, Y.-N.; Liang, H. Organometallic gold (III) complexes similar to tetrahydroisoquinoline induce ER-stress-mediated apoptosis and pro-death autophagy in A549 cancer cells. *J. Med. Chem.* **2018**, *61*, 3478−3490.
(63) Zhang, J.; Zhang, Z.; Jiang, M.; Li, S.; Yuan, H.; Sun, H.; Yang, F.; Liang, H. Developing a novel gold (III) agent to treat glioma based on the unique properties of apoferritin nanoparticles: inducing lethal autophagy and apoptosis. *J. Med. Chem.* **2020**, *63*, 13695−13708.
(64) Alhoshani, A.; Sulaiman, A. A.; Sobeai, H. M. A.; Qamar, W.; Alotaibi, M.; Alhazzani, K.; Monim-ul-Mehboob, M.; Ahmad, S.; Isab, A. A. Anticancer activity and apoptosis induction of Gold (III) complexes containing 2, 2′-bipyridine-3, 3′-dicarboxylic acid and dithiocarbamates. *Molecules* **2021**, *26*, 3973.
(65) Yang, W.; Soares, J.; Greninger, P.; Edelman, E. J.; Lightfoot, H.; Forbes, S.; Bindal, N.; Beare, D.; Smith, J. A.; Thompson, I. R.; Ramaswamy, S.; Futreal, P. A.; Haber, D. A.; Stratton, M. R.; Benes, C.; McDermott, U.; Garnett, M. J. Genomics of Drug Sensitivity in Cancer (GDSC): a resource for therapeutic biomarker discovery in cancer cells. *Nucleic Acids Res.* **2012**, *41*, D955−D961.
(66) Stompor, M.; Świtalska, M.; Wietrzyk, J. The influence of a single and double biotinylation of xanthohumol on its anticancer activity. *Acta Biochim. Pol.* **2019**, *66*, 559−565.
(67) Daina, A.; Michielin, O.; Zoete, V. SwissADME: a free web tool to evaluate pharmacokinetics, drug-likeness and medicinal chemistry friendliness of small molecules. *Sci. Rep.* **2017**, *7*, 42717.
(68) Parkin, S.; Hope, H. Macromolecular Cryocrystallography: Cooling, Mounting, Storage and Transportation of Crystals. *J. Appl. Crystallogr.* **1998**, *31*, 945−953.
(69) Hope, H. X-ray crystallography − a fast, first-resort analytical tool. *Prog. Inorg. Chem.* **2007**, *41*, 1−19.
(70) Bruker *APEX2*; Bruker-AXS, 2006.
(71) Krause, L.; Herbst-Irmer, R.; Sheldrick, G. M.; Stalke, D. Comparison of silver and molybdenum microfocus X-ray sources for single-crystal structure determination. *J. Appl. Crystallogr.* **2015**, *48*, 3−10.
(72) Sheldrick, G. M. SADABS, Program for bruker area detector absorption correction; **1997**.
(73) Sheldrick, G. M. Crystal structure refinement with SHELXL. *Acta Crystallogr., Sect. C: Struct. Chem.* **2015**, *71*, 3−8.

https://doi.org/10.1021/acs.jmedchem.3c00238
J. Med. Chem. 2023, 66, 7868−7879

(74) Sheldrick, G. M. SHELXT − integrated space-group and crystal-structure determination. *Acta Crystallogr., Sect. A: Found Adv.* **2015**, *71*, 3−8.
(75) Sheldrick, G. A short history of SHELX. *Acta Crystallogr., Sect. A: Found Adv.* **2008**, *64*, 112−122.
(76) Spek, A. L. Structure validation in chemical crystallography. *Acta Crystallogr., Sect. D: Biol. Crystallogr.* **2009**, *65*, 148−155.
(77) Parkin, S. Expansion of scalar validation criteria to three dimensions: the R tensor. Erratum. *Acta Crystallogr., Sect. A: Found Adv.* **2000**, *56*, 317.

https://doi.org/10.1021/acs.jmedchem.3c00238
J. Med. Chem. 2023, 66, 7868−7879